Design of the mirror optical systems for coherent diffractive imaging at the SPB/SFX instrument of the European XFEL

2016 J. Opt. 18 074011

(http://iopscience.iop.org/2040-8986/18/7/074011)

OPEN ACCESS
IOP Publishing
Journal of Optics
J. Opt. 18 (2016) 074011 (10pp)
doi:10.1088/2040-8978/18/7/074011

Design of the mirror optical systems for coherent diffractive imaging at the SPB/SFX instrument of the European XFEL

Richard J Bean[1,3], Andrew Aquila[2], Liubov Samoylova[1] and Adrian P Mancuso[1]

[1] European XFEL GmbH, Albert-Einstein-Ring 19, Hamburg, D-22671, Germany
[2] Linac Coherent Light Source, SLAC National Accelerator Laboratory, 2575 Sand Hill Road, Menlo Park, CA 94025, USA

E-mail: richard.bean@xfel.eu

Received 12 January 2016, revised 13 April 2016
Accepted for publication 18 April 2016
Published 6 June 2016

Abstract

The high degree of spatial coherence and extreme pulse energies available at x-ray free electron laser (XFEL) sources naturally support coherent diffractive imaging applications. In order to optimally exploit these unique properties, the optical systems at XFELs must be highly transmissive, focus to appropriate sizes matched to the scale of samples to be investigated and must minimally perturb the wavefront of the XFEL beam. We present the design and simulated performance of two state-of-the-art Kirkpatrik–Baez mirror systems that form the primary foci of the single particles, clusters and biomolecules and serial femtosecond crystallography (SPB/SFX) instrument of the European XFEL. The two systems, presently under construction, will produce 1 μm and 100 nm scale foci across a 3–16 keV photon energy range. Targeted applications include coherent imaging of weakly scattering, often biological, specimens.

Keywords: x-ray optics, coherent diffractive imaging, single particle imaging, serial femtosecond crystallography

(Some figures may appear in colour only in the online journal)

1. Introduction

The single particles, clusters, and biomolecules and serial femtosecond crystallography (SPB/SFX) instrument of the European x-ray free electron laser (XFEL) is designed to perform both single particle imaging (coherent diffractive imaging, or CDI) [1] and serial crystallography [2]. As CDI at XFEL sources is typically a destructive measurement [3, 4], optical systems for such measurements must ideally bring as many x-ray photons in a single XFEL pulse to the sample as possible. This implies a highly transmissive optical system, as well as best matching the spot size on the sample to the sample's size, so photons are not 'wasted' overilluminating the sample. Furthermore, as CDI is an *imaging* technique, the wavefront of the illumination incident upon the sample must either be uniform across the length scale of the sample, or characterisable.

This paper describes the optical system of the under-construction SPB/SFX instrument of the European XFEL, and how the questions of transmission, spot size and wavefront quality have been addressed. Calculated system transmissions are shown, as well as simulated images of focused beam transverse structure using example FEL performance parameters.

1.1. European XFEL

The European XFEL is an XFEL source based on a superconducting linear accelerator. Initially, three (3) undulators

[3] Author to whom any correspondence should be addressed.

will generate x-ray pules for experiments at six (6) instruments with two (2) instruments located on each undulator beamlime. The European XFEL operates with a 10 Hz pulse train bunch structure. Each pulse train can be filled with up to 2700 bunches. Individual x-ray pulses will be of order 10 fs in duration, contain a few mJ of energy, and will be separated by 220 ns (4.5 MHz). This structure provides not only very high peak brilliance, but also the highest average brilliance of any x-ray FEL. The x-ray beam is expected to be highly spatially coherent [5], with the degree of coherence decreasing for harder-energy x-rays or higher bunch charge in the accelerator (higher photon flux).

1.2. The SPB/SFX instrument

The SPB/SFX instrument is located on the centre beamline behind the SASE1 undulator of the European XFEL [6]. The instrument is primarily concerned with three-dimensional imaging, or three-dimensional structure determination, of micrometer-scale and smaller objects. A particular emphasis is placed on biological systems, including viruses, biomolecules, and protein crystals, though the instrument will also be capable of investigating non-biological samples using similar techniques. It is expected that forming molecular movies [7] using nanocrystallography [8] or single particle imaging [1, 9] techniques will make up the majority of experiments at the SPB/SFX instrument.

In order to accommodate the range of expected sample sizes and sampling conditions required for diffraction experiments, two focal spot sizes will be available at a common focal plane. The two spot sizes are 1 μm scale and 100 nm scale, with the energy dependent exact size limited by the numerical aperture of the optics. The primary goals of the optical system of the SPB/SFX instrument are to deliver the maximum number of photons to the interaction region across the operating photon energy range of the instrument (3–16 keV), and produce a flat, uniform, or characterisable wavefront in the focal plane.

SPB/SFX is a high vacuum, window-less instrument, intended to provide a flexible experimental environment for a variety of sample delivery techniques. The European XFEL's pulse train structure is well suited for samples delivered via aerosol injection [9], and is also compatible with liquid injection techniques [10]. This allows the sample to be replenished on an appropriate timescale to take advantage of the maximal 4.5 MHz rate provided by the accelerator.

Diffracted photons are collected by a two-dimensional 1 megapixel adaptive gain integrating pixel detector (AGIPD) [11], capable of recording single x-ray pulses at the full 4.5 MHz repetition rate, and retaining on the order of 350 patterns for analysis. Fast veto systems are currently under development to maximise the useful data rate. The detector position can be varied from 13 cm to 5 m downstream of the common focal plane.

A second, fully integrated interaction region contributed by the serial femtosecond crystallography users' consortium [12] will be installed downstream of the primary focus. Under a range of operational conditions, the x-ray FEL radiation transmitted through the upstream interaction region will be refocused into this sample chamber using a beryllium compound refractive lens stack to allow the simultaneous operation of serial crystallography experiments. The optical design provides a 1:1 focus position for the lens stack with scope for translation to optimise the focus given discrete lens options.

1.3. Coherent optics

Important to the technique of single particle imaging, and CDI in general, is the use of a coherent source. In addition to coherence, a minimally perturbed wavefront of the x-ray FEL beam is desirable. For coherent diffractive techniques to work efficiently and accurately, the wavefront incident on a sample needs to be well-characterized and incorporated into the phase retrieval procedure [13]. A slowly varying field, such as a Gaussian beam or plane wave front, greatly improves the ability to reconstruct the object illuminated from the field [14]. Therefore any optical system selected for an endstation specialising in coherent imaging needs to have wavefront preserving properties.

2. Optical layout

2.1. Overview

The location of the SPB/SFX instrument on the centre beamline of the SASE1 undulator minimises the number of optical elements between the source point and instrument focusing optics. The optical layout has been designed according to the simulated behavior of the accelerator and undulator system under standard operation, i.e. without oversaturation or tapering [15]. The SASE1 source point is estimated to be located in the second-to-last undulator section, 918 $\pm$ 2 m from the common focal plane of the upstream interaction region. It is estimated that the x-ray beam at the source point will have a diameter of 33 $\pm$ 5 μm FWHM at the minimum bunch charge of 0.02 nC and 53 $\pm$ 10 μm at the maximum bunch charge of 1 nC across the SPB/SFX operation energy range with standard operation of the accelerator. The source size varies only slightly with accelerator energy and decreases somewhat with reduced electron bunch charge. The divergence is expected to vary between 6 μrad at the lowest photon energies and 1 μrad at the highest photon energies. Further information on expected source parameters can be found in [15]. Due to the long propagation distance, moderate deviation of the photon source point from the expected value in other accelerator modes is not expected to adversely effect the performance of the optical systems.

A pair of B_4C coated flat offset mirrors, centred 680 m upstream of the instrument common focal plane, are installed for radiation protection. These mirrors remove high-energy Bremsstrahlung and spontaneous undulator radiation co-propagating with the desired FEL beam with an energy cut-off at 24 keV.

The high repetition rate and high peak fluence of the FEL combined with the expected divergence and long 900 m propagation distance provide a challenging set of constraints for the design of the instrument optical system. Typical x-ray

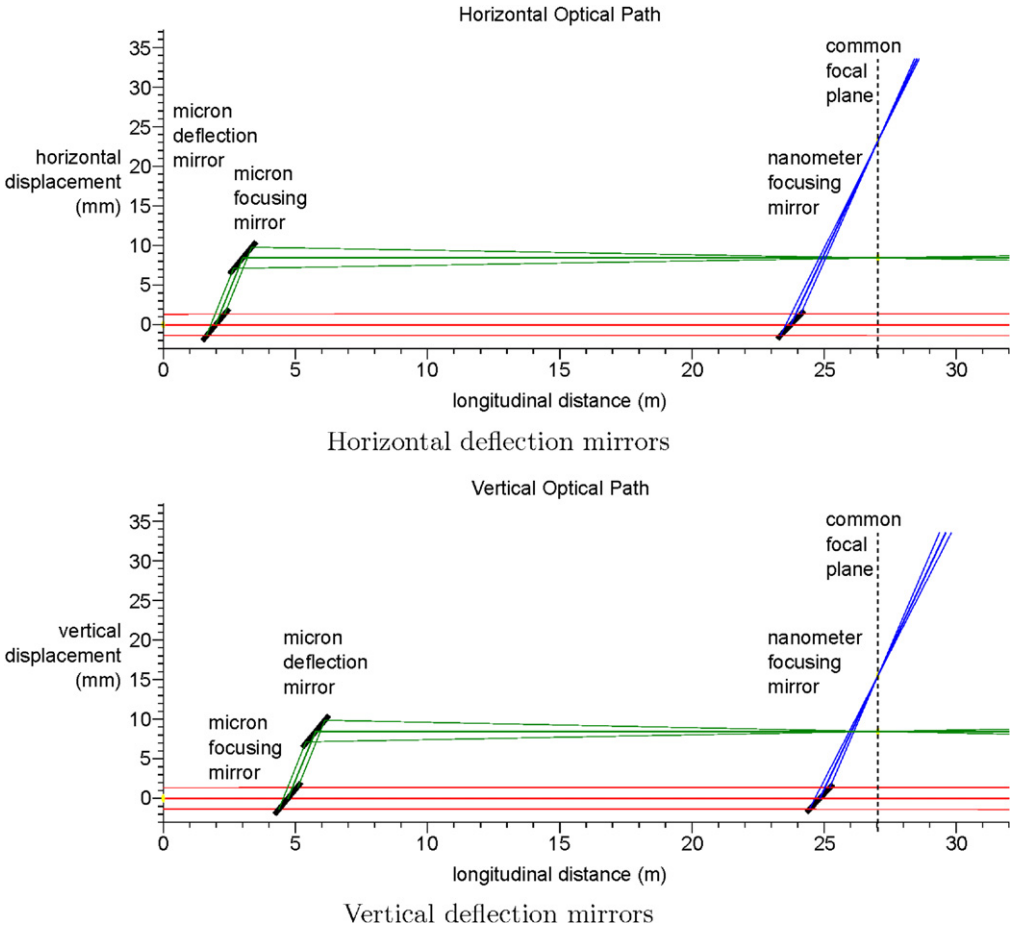

Figure 1. Representation of the optical layout of the SPB/SFX instrument, showing horizontally deflecting mirrors in panel 1 and vertically deflecting mirrors in panel 2. The incident beam into the instrument is represented in red, with the 1 μm scale system in green and the 100 nm scale system in blue. The 0 m mark in the longitudinal distance represents the beginning of the experimental floor. The three lines represent the central and extreme rays from the source at 8 keV, assuming upper limits for source size and divergence according to [15]. The horizontally deflecting flat mirror and horizontal elliptical focusing mirror, of the four bounce, 1 μm scale KB focusing system are mounted in a vacuum tank in the optics hutch, centred 25.055 and 24.005 m upstream of the common focal plane respectively. The vertical elliptical focusing mirror and vertically deflecting flat mirror, also of the four bounce, 1 μm scale KB focusing system are mounted in a second vacuum tank in the optics hutch, centred 22.325 and 21.275 m upstream of the common focal plane respectively. The two KB mirrors of the 100 nm scale system share a vacuum tank, with the horizontally and vertically focusing optics centred at 3.300 and 2.200 m upstream of the common focal plane respectively.

beam sizes at the entrance to the instrument range from 1 to 6 mm FWHM, requiring large apertures to obtain diffraction limited foci.

The upstream interaction region of the SPB/SFX instrument will use Kirkpatrick–Baez (KB) mirrors [16] for focusing the XFEL radiation into both the 1 μm scale and 100 nm scale foci. KB mirrors are elliptically curved grazing incidence mirrors where the source point and the x-ray focus form the two foci of the ellipse. KB optics were chosen as the only viable solution as large aperture sizes and high system efficiencies are possible, with the ability to survive the pulse structure and the additional advantages of being achromatic and wavefront preserving. The location of the two sets of KB optics required are fully determined by geometrical optics arguments, considering the source size, desired focal sizes, and the source-to-focus distance. Specifics of the KB systems designed for the 1 μm scale and 100 nm scale foci are described in the following sections.

2.2. μm-scale focus

The geometrical centre of the 1 μm scale focusing optics lies 23.2 m upstream of the common focal plane and 894.8 m from the expected source point. Due to the divergence of the source resulting in large beam sizes at this position, a large clear aperture is required, especially at lower energies. The KB design therefore incorporates a relatively high incidence angle of 4 mrad with 1000 mm silicon substrate mirrors. A 950 mm $\times$ 25 mm ultra highly polished central region, the limit of current fabrication capability, results in a maximum aperture of 3.8 mm. A traditional 2-mirror KB pair at this distance from the focal plane would result in a large beam deviation at the focal plane of up to 300 mm both vertically and horizontally. Instead, a 4 bounce solution is implemented as shown in figure 1. A four bounce design has a number of advantages, including reduced sensitivity to incident beam position variation (that is, improved vibrational tolerance). Variations in position, of either the mirrors themselves or the

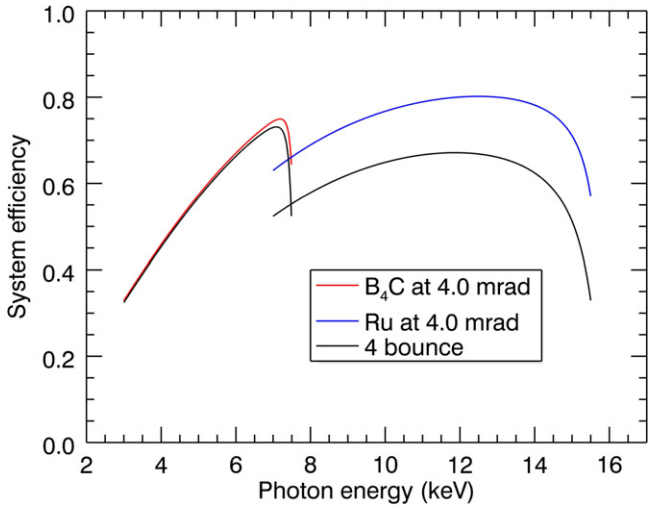

Figure 2. Total predicted transmitted efficiency for the 1 μm scale focusing system as a function of energy, including the energy dependent, aperture limited acceptance. The chosen 4 bounce system, black line, is compared with a two bounce system for both B_4C, red line, and Ru, blue line, coatings.

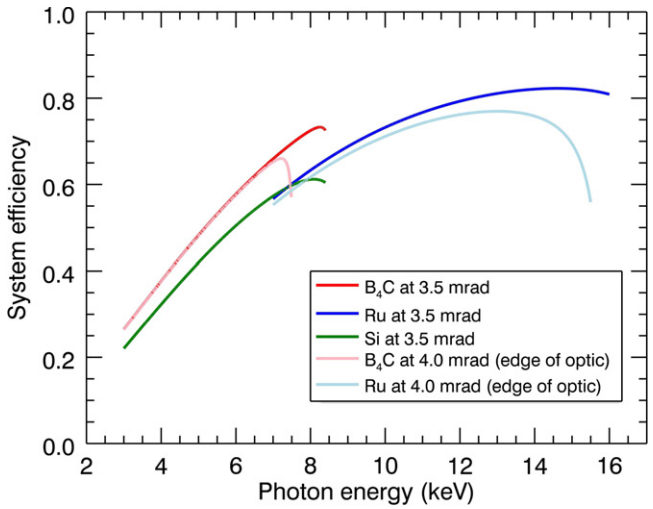

Figure 3. Total predicted transmitted efficiency for the 100 nm scale focusing system as a function of energy, including the energy dependent, aperture limited acceptance. The transmission at the centre (downstream edge) of the two bounce system is shown for the B_4C, red (pink) line, and the Ru, blue (light blue), coatings. The transmission of the bare Si substrate, green, is shown for comparison.

incident beam, do not map to angular variation in the focused beam and instead result in intensity fluctuations. The outgoing beam of the 4 bounce system is parallel to the incident beam, with only a small horizontal and vertical offset of 8.4 mm introduced, reducing the complexity of design requirements on the 100 nm scale KB optical system and other downstream instrumentation. Upgrade possibilities are also envisaged, with the potential ability to adjust the wavefront by actuation of the flat deflection mirrors [17]. A four bounce system, with a high incidence angle, provides excellent harmonic rejection at the cost of overall transmission and possible additional wavefront degradation compared to a 2 bounce system.

The four (4), 1000 mm, 1 μm scale mirrors are housed in two (2) vacuum tanks in the SPB/SFX optics hutch. The flat horizontal deflection mirror is the most upstream, followed by the horizontal focusing KB, centred 24.005 m from the focus. The upward facing vertical focusing KB is the most upstream mirror in the second tank, centred 22.325 m from the focus, followed by the downward facing flat vertical deflection mirror. Mirror specifications including the shape defining parameters and controlled axes are shown for the system in table 1.

At 8 keV, the depth of focus of the 1 μm scale system is expected to be 11.36 mm, with the exact observed value changing with the energy-dependent divergence of the source, given the fixed aperture of the optical system.

2.3. 100 nm scale focus

The geometrical centre of the 100 nm scale KB optics lies 2.75 m from the common focal plane and 915.25 m from the SASE1 undulator expected source point. Similar to the 1 μm scale case, the large beam sizes at the entrance to the optics require a large clear aperture. Again, 1000 mm silicon-substrate mirrors with 950 mm ultra-polished central region are selected. As the optics are approximately a factor of 10 closer to the common focal plane than the μ-scale pair, the 100 nm-scale optics have a much larger curvature. To limit the incidence angle to the same, 4 mrad, maximum at the downstream end of the mirrors, the incidence angle at the centre of the mirrors is limited to 3.5 mrad with a consequent reduction in aperture to 3.3 mm.

The KB pair are arranged so that the focused beam is deflected in the same direction as the offset produced by the 1 μm scale system. The mirrors are housed in a single vacuum tank, located directly upstream of the interaction region chamber in the SPB/SFX experiment hutch, as indicated in figure 1. The horizontal mirror is the most upstream of the pair. A differential pumping section protects the vacuum in the mirror tank from sample injection in the interaction chamber. Mirror specifications including the shape defining parameters and controlled axes are shown for the system in table 2.

At 8 keV, the depth of focus of the 100 nm scale system is expected to be 0.17 mm, with the exact observed value changing with the energy dependent divergence of the source, given the fixed aperture of the optical system.

All mirrors are currently in fabrication at JTEC, Osaka, Japan, with positioning system, cooling and vacuum chamber designed and manufactured by FMB-Oxford, Oxford, UK.

2.4. Optical coatings

The high incidence angles required to achieve an acceptable aperture, and the desired energy operation range of the SPB/SFX instrument from 3 to 16 keV, has strongly influenced our decision to use a metal coating with a higher critical angle than the traditional low-*Z* materials used at existing hard x-ray FEL facilities [18, 19]. To minimise the harmonic content of

Table 1. Table of specifications for all four mirrors of the 1 μm scale optical system.

MHP	Micron horizontal plane mirror
Deflection	Horizontal (positive x)
Meridonial radius (minimum)	500 km
Saggital radius (minimum)	10 km

Controlled motion (relative to incident beam)	Minimum	Maximum	Resolution
X	−10 mm	+2 mm	<1 μm
Y (coating selection)	−15 mm	+15 mm	<1 μm
θ_y (pitch)	−0.5 mrad	+5.5 mrad	<20 nrad

MHE	Micron horizontal elliptical KB
Deflection	Horizontal (negative x)
Source—optic (centre) distance	894.779 m
Optic (centre) focus distance	24.005 m
Saggital radius (minimum)	10 km

Controlled motion (relative to incident beam)	Minimum	Maximum	Resolution
X	−2 mm	+10 mm	<1 μm
Y (coating selection)	−15 mm	+15 mm	<1 μm
θ_y (pitch)	−0.5 mrad	+5.5 mrad	<20 nrad

MVE	Micron vertical elliptical KB
Deflection	Vertical (positive y)
Source—optic (centre) distance	896.459 m
Optic (centre) focus distance	22.325 m
Saggital radius (minimum)	10 km

Controlled motion (relative to incident beam)	Minimum	Maximum	Resolution
X (coating selection)	−15 mm	+15 mm	<1 μm
Y	−10 mm	+2 mm	<1 μm
θ_x (pitch)	−5.5 mrad	+0.5 mrad	<20 nrad
θ_y (yaw)	−5 mrad	+5 mrad	<1 μrad
θ_z (roll)	−5 mrad	+5 mrad	<1 μrad

MVP	Micron vertical plane mirror
Deflection	Vertical (negative y)
Meridonial radius (minimum)	500 km
Saggital radius (minimum)	10 km

Controlled motion (relative to incident beam)	Minimum	Maximum	Resolution
X (coating selection)	−15 mm	+15 mm	<1 μm
Y	−2 mm	+10 mm	<1 μm
θ_x (pitch)	−5.5 mrad	+0.5 mrad	<20 nrad
θ_y (yaw)	−5 mrad	+5 mrad	<1 μrad
θ_z (roll)	−5 mrad	+5 mrad	<1 μrad

Table 2. Table of specification for the two mirrors of the 100 nm scale optical system.

NHE	Nanometer horizontal elliptical KB
Deflection	Horizontal (positive x)
Source—optic (centre) distance	915.484 m
Optic (centre) focus distance	3.3 m
Saggital radius (minimum)	10 km

Controlled motion (relative to incident beam)	Minimum	Maximum	Resolution
X	−10 mm	+5 mm	<1 μm
Y (coating selection)	−15 mm	+15 mm	<1 μm
Z (astigmatism correction)	−5 mm	+5 mm	<1 μm
θ_y (pitch)	−0.5 mrad	+5.5 mrad	<20 nrad

NVE	Nanometer vertical elliptical KB
Deflection	Vertical (positive y)
Source—optic distance	916.584 m
Optic—focus distance	2.2 m
Saggital radius (minimum)	10 km

Controlled motion (relative to incident beam)	Minimum	Maximum	Resolution
X (coating selection)	−15 mm	+15 mm	<1 μm
Y	−10 mm	+5 mm	<1 μm
Z (astigmatism correction)	−5 mm	+5 mm	<1 μm
θ_x (pitch)	−5.5 mrad	+0.5 mrad	<20 nrad
θ_y (yaw)	−5 mrad	+5 mrad	<1 μrad
θ_z (roll)	−2 mrad	+2 mrad	<1 μrad

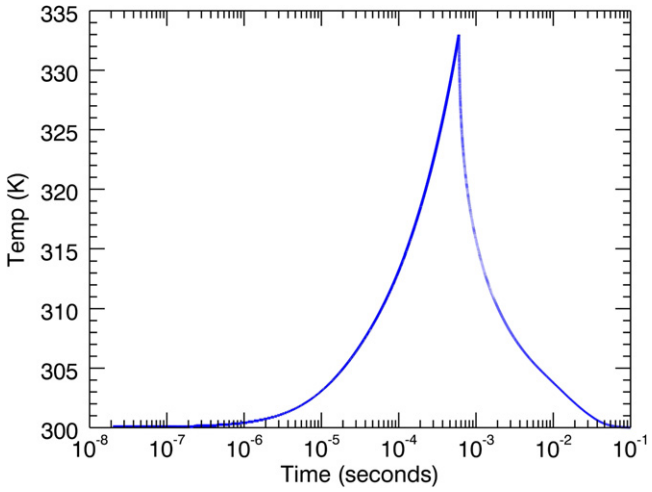

Figure 4. The plot shows the maximum temperature of the 50 nm Ru capping layer on a Si substrate, as a function of time. The simulation is formed from a 3D finite difference analysis of the heat transport through the KB mirror averaged over the centre 15 mm by 0.5 mm area. The Si voxels had a volume of 32 mm^3 and covered the entire optic. The simulation used a full pulse train of 2700 pulses at 4.5 MHz with 1 mJ per pulse. While the heat reached a peak of 33 ° K above room temperature, it cools back down within the 10 Hz pulse train window (time shown on a logarithmic scale). This assumes a heat bath surrounding the optics.

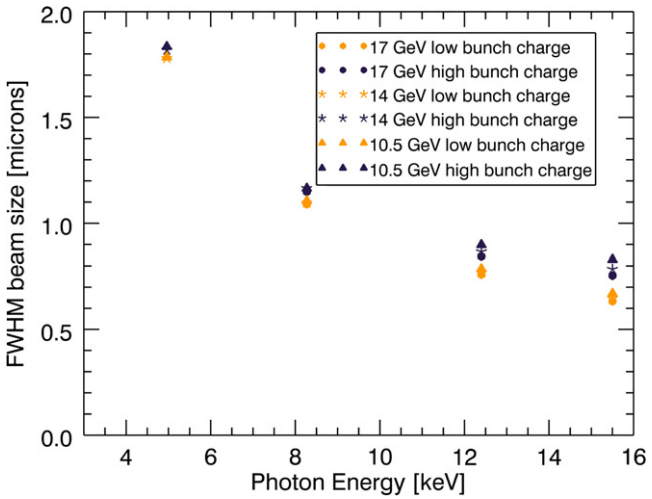

Figure 5. Estimations of the full width at half max. X-ray focal spot size for the micron-scale focus under various electron beam conditions. Low and high bunch charges refer to 0.02 nC and 1 nC respectively. Calculations assume a perfect Gaussian beam. The variation in focus size at higher photon energies is due to changes in source size as a function of bunch charge, this effect is reduced at lower photon energies where the x-ray beam is numerical aperture limited.

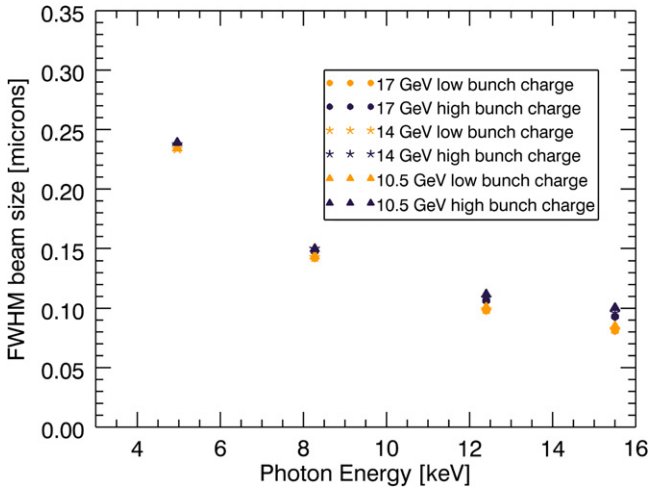

Figure 6. Estimations of the full width at half max x-ray focal spot size for the 100 nm scale focus under various electron beam conditions. Low and high bunch charges refer to 0.02 nC and 1 nC respectively. Calculations assume a perfect Gaussian beam. The variation in focus size at higher photon energies is due to changes in source size as a function of bunch charge, this effect is reduced at lower photon energies where the x-ray beam is numerical aperture limited.

the beam, two (2) coatings will be applied to each of the six (6) mirrors in the SPB/SFX focusing setup. A 10 mm stripe of each coating will be applied side-by-side to all mirrors over the complete super-polished length. The relevant coating is selected before operation though translation of the optic in the relevant axis.

Boron carbide (B_4C) will be used from 3 to 7.5 keV and ruthenium (Ru) from 7.5 to 16 keV, eliminating the second, and higher harmonics over most of the operating range. Metal coatings, such as Ru, provide higher critical angles (larger numeric aperture for the same mirror length) and a less sharp loss of reflectivity at the critical angle, with a cost of stronger absorption at the surface of the mirror. Higher absorption could lead to coating damage if the x-ray fluence were large enough. Measurements have therefore been conducted on both B_4C and Ru coatings to determine their damage threshold fluence [20], and this showed that both coatings are expected to survive under the operating conditions at the SPB/SFX instrument.

The predicted overall efficiencies of the 1 μm scale and 100 nm scale optics, with the optical coatings applied, and taking into account the aperture limited acceptance, are shown in figures 2 and 3 as a function of photon energy. In the 1 μm scale case, figure 2, the total reflectivity for the designed four-bounce system is shown, with the efficiency of a two-bounce system shown for comparison. In the 100 nm case, figure 3, the efficiency in the centre of the optics, at 3.5 mrad is compared with that at 4 mrad at the downstream end of the optics. The bare Si substrate transmission is also shown, demonstrating the reflectivity improvement of the B_4C coating for low energies.

2.5. Thermal loads

In addition to the concerns regarding coating ablation discussed above and in [20], an additional concern is the dramatic changes in the thermal loading on the coatings during a pulse train due to the 4.5 MHz pulse train structure. While each pulse results in less than 50 μJ of energy absorbed in the mirrors, the pulse train bunch pattern, with up to 2700 pulses per train, might cause the surface to significantly deform or melt by the end of the pulse train. This is especially a concern for the Ru coating, where the absorption length is significantly less than that of B_4C. The thermal load absorbed in the mirror follows the truncated Gaussian distribution of the beam in both transverse and longitudinal directions. Temperature gradients on the mirror surface are also a potential source of figure aberrations.

Simulations of the heat load on a 50 nm Ru coating of a Si mirror during a full pulse train of 2700 pulses are shown in figure 4. The simulation calculates a 33 K rise in the temperature of the coating by the end of the pulse train, with pulses of 1 mJ, and returning to the original temperature within the 600 μs between the pulse trains. Calculations for B_4C have also been conducted; however, as the reflectivity is nearly 99% up to its critical angle, the coating is expected to be significantly further from melting or deformation limits.

To allow these modest heat loads to be removed from the optical system and to provide scope for possible upgrades, all mirrors are thermally stabilised using vibrationally isolated copper blades, suspended in indium–gallium coolant channels. Heat is removed from the copper blades by a combination of thermoelectric and water-cooling. At the time of writing, the cooling system is in the testing phase and a further publication with details of design and observed performance is expected at a later date.

3. Implications of coherence on mirror design

3.1. Wavefront truncation

As mentioned in section 2.4 the most significant loss of power, especially at lower photon energies, is the limited clear aperture or numerical aperture of the x-ray optical system. The truncation of the propagating wavefront leads to diffraction effects, fringes, in the focal plane and a larger focal spot, diffraction limited, than that calculated by geometric optics alone. These effects are well documented in the study of laser diffraction theory [21, 22].

A truncation ratio can be used to estimate the spot size, peak spot intensity and power loss of a coherent optical system. Reasonable trade offs between peak spot intensity and focal size have truncation ratios between 0.7 and 1.0 [23]. Assuming a perfect Gaussian beam, it is estimated that the SPB/SFX KB systems will have a truncation ratio greater than 2 below 4 keV, decreasing to 1 at 10 keV and falling to 0.7 at 16 keV.

More detailed approximations have been conducted using expected beam sizes [15] and numerical approximations for truncations of a focusing wavefront [24] and are shown in figure 5 for the micron-scale focus and figure 6 for the 100 nm scale focus.

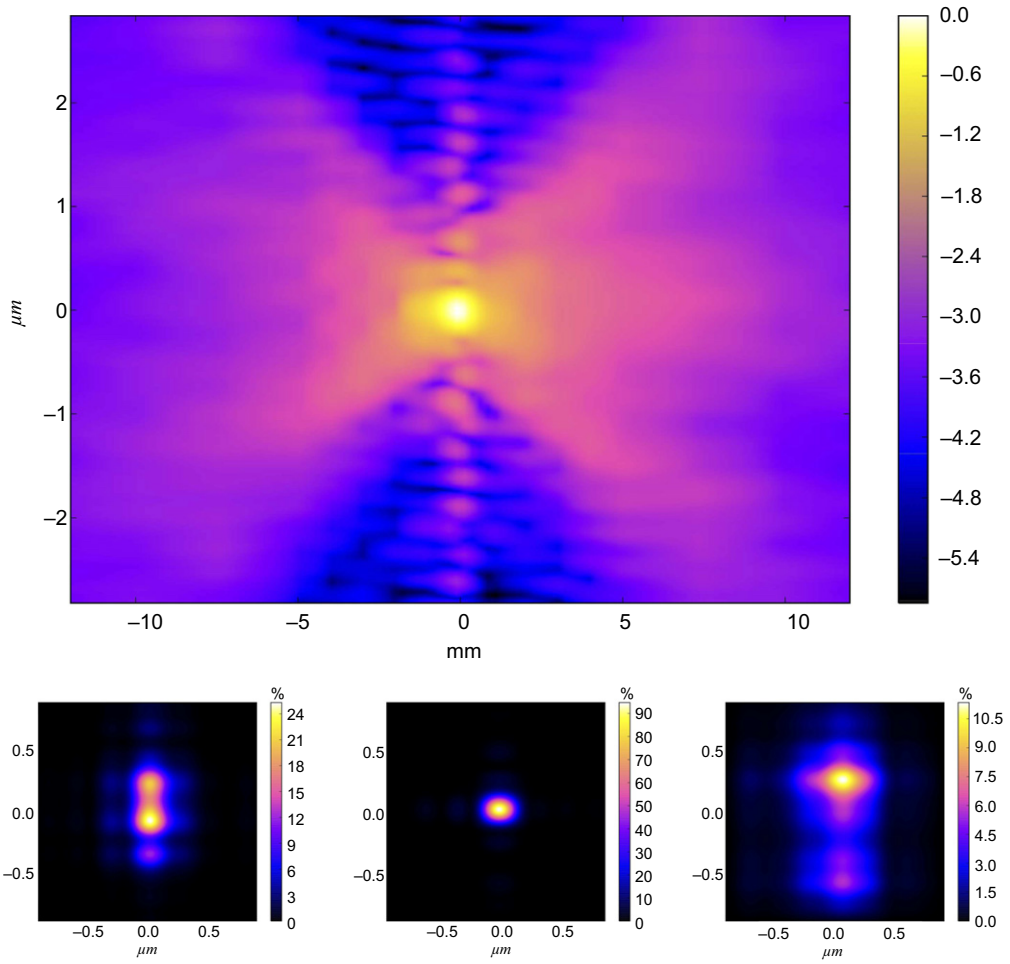

Figure 7. Simulated intensity distribution of the SPB/SFX 100 nm scale focus (see main text for details). Top panel: intensity distribution in instrument '*xz*' plane (through focus), normalised to the highest intensity observed in the simulation and shown on a log scale. Propagation direction is left to right. Lower panel: intensity distribution in the plane perpendicular to the direction of propagation, normalised to the highest intensity observed in the simulation and displayed as a percentage of that maximum. Cuts of the intensity distribution are shown at 5 mm upstream of the focus (left), in the focal plane (centre), and 5 mm downstream of the focus (right).

Table 3. Table of surface quality specifications applicable to all six mirrors of the instrument.

Error category	Spatial frequency	length-scale	Specification
High spatial frequency	0.5 μm^{-1}–50.0 μm^{-1}	20 nm–2 μm	<0.4 nm rms
Mid spatial frequency	100 m^{-1}–0.5 μm^{-1}	2 μm–10 mm	<0.25 nm rms
figure (slope errors)	100 m^{-1}–1.0 m^{-1}	10 mm–1 m	<20 nrad rms
Residual height errors	100 m^{-1}–1.0 m^{-1}	10 mm –1 m	<0.5 nm rms

3.2. Figure error and roughness

Even with state-of-the-art polishing techniques, no optic can be considered as an ideal optic. The figure and finish of an optic are critical to its performance [25]. A large body of literature has been built on the specification of slope and height errors [26, 27], as well as metrology to measure these errors [28]. In addition to shape errors, high spatial frequency height errors, or roughness, are known to lead to significant tails or halo around the focal spot [29, 30].

The power spectral density is often used to describe a mirror system's performance: focal spot size and wavefront. While the exact fractal dimension of the shape can be specified, often the maximum slope error and rms height error as well as mid and high spatial frequency roughness are typically specified. Due to the long working distance of 25 m for the micron-scale focus, the slope errors need to be better than 0.02 μrad [25]. Using the Strehl relation for the high spatial frequencies, roughness needs to be better than 1 nm rms, while the Marechal criterion gives a required figure error of less than 0.6 nm rms for a four-bounce optical system [28]. If we include the two offset mirrors in the total mirror count, there is a consequent increase in specification of the rms height error. If the roughness specification is set to the standard for current state-of-the-art synchrotron optics, this factor of 2.5 reduction has the effect of reducing

the deterioration of peak intensity, caused by roughness, by 85% (a 10% loss compared to a 1.7% absolute loss in peak efficiency per optic). We note that the slope error specification will only reduce the peak brightness by 0.1% (per optic); however, slope errors cause the beam distribution and tails to deviate from a Gaussian profile and distort the wavefront [27]. As a primary goal of our scientific instrument is imaging, any deviation could potentially complicate reconstructions. A table of surface quality specifications is given in table 3.

3.3. Wavefront simulations

Detailed simulations provide an informative analysis of the intensity distribution reaching the common focal plane, accounting for the FEL source and the KB focusing optics. The simulated intensity distribution around the common focal plane for the SPB/SFX 100 nm scale KB system is presented here. Wavefront propagation was performed in the WPG framework [31], using the near field approach implemented in the Synchrotron Radiation Workshop library [32]. We use the FAST code data from x-ray photon pulses database (XPD) [33] to describe the European XFEL source. Figure 7 shows the intensity distribution around the focal spot of the 100 nm scale KB optics for a single SASE pulse. Slices of the intensity distribution in the lower panel of figure 7 correspond to the intensity of the whole pulse at the focal plane and 5 mm upstream and downstream of the focal plane as it would be registered by a 2D detector. Parameters used for the simulation are a short, 3 fs FWHM SASE pulse with a 20 pC electron bunch charge, an average photon energy of 4.96 keV and an active undulator length of 105 m. Profile error maps with peak-to-valley height errors of 3 nm are applied to all four (4) mirrors on the optical path, two (2) offset mirrors and the KB pair of the 100 nm system.

The simulated wavefront in figure 7, shows fringe features both in the focal plane and out-of-focus, as expected from the truncation of the propagated wavefront and estimated deviations from the ideal optical surface specifications. Features similar to those seen in this simulation have been observed at other x-ray FEL instruments [34, 35]. With a well characterised focus, fringes in the focal plane are not considered to be problematic for image reconstruction [36, 37]. Nevertheless, several sets of slits between the optics and focal plane are foreseen including directly upstream of the focus inside the interaction region chamber.

4. Conclusion

The SPB/SFX primary foci design uses state-of-the-art mirror systems with the goal of producing a highly transmissive optical system, with as well-defined and characterisable an XFEL beam as possible for imaging applications. The two focal spot size ranges address the breadth of samples expected at SPB/SFX, from very sub-100 nm single biomolecules through to viruses, organelles and single cells up to about the micron scale. Wavefront modeling, particularly relevant for the highly coherent beams produced by XFELs, has been used to ensure the mirror design meets these requirements. The exquisite figure error specified for the mirrors currently in fabrication as well as their unprecedented aperture, due to their length and incidence angles achieved by B_4C and Ruthenium coatings, suggest this optical system will deliver high quality XFEL beams across the 3–16 keV photon energy range.

References

[1] Aquila A *et al* 2015 *Struct. Dyn.* **2** 041701
[2] Chapman H N *et al* 2011 *Nature* **470** 73–7
[3] Chapman H N *et al* 2006 *Nat. Phys.* **2** 839–43
[4] Neutze R, Wouts R, van der Spoel D, Weckert E and Hajdu J 2000 *Nature* **406** 752–7
[5] Geloni G, Saldin E, Samoylova L, Schneidmiller E, Sinn H, Tschentscher T and Yurkov M 2010 *New J. Phys.* **12** 035021
[6] Mancuso A, Aquila A, Borchers G, Reimers N and Giewekemeyer K 2013 Technical design report scientific instrument single particles, clusters, and biomolecules (spb) *Technical Report* TR-2013-004 (doi:http://dx.doi.org/10.3204/XFEL.EU/TR-2013-004)
[7] Barty A, Küpper J and Chapman H N 2013 *Annu. Rev. Phys. Chem.* **64** 415–35
[8] Boutet S *et al* 2012 *Science* **337** 362–4
[9] Seibert M M *et al* 2011 *Nature* **470** 78–81
[10] DePonte D P, Weierstall U, Schmidt K, Warner J, Starodub D, Spence J C H and Doak R B 2008 *J. Phys. D: Appl. Phys.* **41** 195505
[11] Henrich B *et al* 2011 *Nucl. Instrum. Methods Phys. Res.* A **633** (Suppl. 1) S11–4 *11th Int. Workshop on Radiation Imaging Detectors (IWORID)*
[12] European XFEL 2016 Web page of user consortia at the European XFEL http://xfel.eu/organization/user_consortia/
[13] Williams G J, Quiney H M, Dhal B B, Tran C Q, Nugent K A, Peele A G, Paterson D and de Jonge M D 2006 *Phys. Rev. Lett.* **97** 025506
[14] Williams G J, Quiney H M, Peele A G and Nugent K A 2007 *Phys. Rev.* B **75** 104102
[15] Schneidmiller E and Yurkov M 2011 Photon beam properties at the European XFEL *Technical Report* TR-2011-006 (doi: http://dx.doi.org/10.3204/DESY11-152)
[16] Kirkpatrick P and Baez A V 1948 *J. Opt. Soc. Am.* **38** 766–74
[17] Yabashi M *et al* 2014 *J. Synchrotron Radiat.* **21** 976–85
[18] Boutet S and Williams G J 2010 *New J. Phys.* **12** 035024
[19] Liang M *et al* 2015 *J. Synchrotron Radiat.* **22** 514–9
[20] Aquila A *et al* 2015 *Appl. Phys. Lett.* **106** 241905
[21] Belland P and Crenn J P 1982 *Appl. Opt.* **21** 522–7
[22] Dickson L D 1970 *Appl. Opt.* **9** 1854–61
[23] Byatt J 2003 Laser beam control *Handbook of Laser Technology and Applications (Three- Volume Set)* (London: Taylor and Francis) pp 135–60 ISBN 978-0-7503-0607-2 http://dx.doi.org/10.1201/NOE0750309608.ch5
[24] Urey H 2004 *Appl. Opt.* **43** 620–5
[25] Church E L and Takacs P Z 1995 *Opt. Eng., Bellingham* **34** 353–60
[26] Yashchuk V V, Samoylova L V and Kozhevnikov I V 2015 *Opt. Eng., Bellingham* **54** 025108
[27] Pardini T, Cocco D and Hau-Riege S P 2015 *Opt. Express* **23** 31889–95

[28] Siewert F, Buchheim J, Boutet S, Williams G J, Montanez P A, Krzywinski J and Signorato R 2012 *Opt. Express* **20** 4525–36
[29] Pivovaroff M J, Bionta R M, Mccarville T J, Soufli R and Stefan P M 2007 Soft x-ray mirrors for the Linac coherent light source *Proc. SPIE* **6705** 67050O
[30] Soufli R *et al* 2008 Development, characterization and experimental performance of x-ray optics for the LCLS free-electron laser *Proc. SPIE* **7077** 707716
[31] Samoylova L, Buzmakov A, Chubar O and Sinn H 2016 WPG-wavepropergator is an interactive simulation framework for coherent x-ray wavefront propagation *J. Appl. Cryst.* submitted
[32] Chubar O, Couprie M E, Labat M, Lambert G, Polack F and Tcherbakoff O 2008 *Nucl. Instrum. Methods Phys. Res.* A **593** 30–4 {*FEL*} *Fronties 2007Proc. Int. Workshop on Frontiers in* {*FEL*} *Physics and Related Topics*
[33] Manetti M *et al* 2015 XFEL photon pulses database (XPD) for modeling x-ray experiments https://in.xfel.eu/xpd
[34] Chalupský J *et al* 2015 *Phys. Rev. Appl.* **4** 014004
[35] Gerasimova N, Dziarzhytski S, Weigelt H, Chalupský J, Hájková V, Vyšín L and Juha L 2013 *Rev. Sci. Instrum.* **84** 065104
[36] Flewett S, Quiney H M, Tran C Q and Nugent K A 2009 *Opt. Lett.* **34** 2198–200
[37] Whitehead L W, Williams G J, Quiney H M, Vine D J, Dilanian R A, Flewett S, Nugent K A, Peele A G, Balaur E and McNulty I 2009 *Phys. Rev. Lett.* **103** 243902